RSC Advances

ROYAL SOCIETY OF CHEMISTRY

www.rsc.org/advances

Table of Contents (TOC)

Flake-like carbon-based iron oxide composites were prepared via hydrothermal reaction followed by a carbonization processes and exhibit excellent recycling durability.

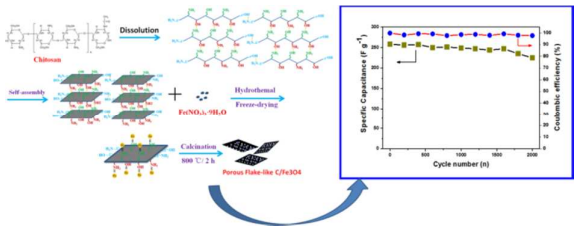

Synthesis of Partially Graphitic Nanoflake-Like Carbon/Fe_3O_4 Magnetic Composite from Chitosan as High-Performances Electrode Materials in Supercapacitor

Mengjiao Wang, Wenhua Wang, Wanren Wang, Xiaohui Guo*

Abstract:

In this study, we report that partially graphitic nanoflake-like carbons derived from chitosan and their magnetic composite were prepared via hydrothermal reaction followed by a high-temperature carbonization process. The prepared iron oxide particles are well dispersed onto the surface of the carbon support and display good single-crystalline feature. In addition, the carbon/iron oxide composite serve as electrode material in supercapacitor. Electrochemical results demonstrated that the carbon/iron oxide based electrode can deliver high specific capacitance ~ 299 F g^{-1} at current density of 0.5 A g^{-1} and excellent recycling durability, which is probably due to the fast electron and ion transport, the enhanced conductivity and the generated pseudocapacitance that resulted from sufficient Faradic redox reaction. More importantly, the present synthetic approach is green and reproducible, which can facilitate to design and fabricate other carbon-based advanced function materials and devices.

---

[*] Dr. Prof. Xiaohui Guo, Dr. Mengjiao Wang, Wenhua Wang, Wanren Wang, Key Lab of Synthetic and Natural Functional Molecule Chemistry of Ministry of Education, the College of Chemistry and Materials Science, Northwest University,

Xi'an 710069, P. R. China. Tel: 86-2988302604. E-mail: guoxh2009@nwu.edu.cn, Tel: (+) 86-29-88302604.

Introduction:

Electrochemical capacitors (ECs) as promising energy-storage devices have dramatically increased applications in such as mobile electronic devices, back-up power supplies, and hybrid electric vehicles due to their fast charging and discharging, long cycle lifetime features.[1-3] Particularly, carbon based electrode materials in ECs have triggered tremendous attention in both theoretical and practical application aspects owing to their high power density, superior performance in extreme temperatures, as well as outstanding cycle stability in the past decades.[4-6]

Currently, nanostructured carbon materials, including activated carbons,[7] porous carbons,[8] carbon nanotubes,[9] carbon fiber,[10] and graphene,[11] have been proved to possess storage-energy performances. Although much attention has been focused on the application of carbon based electrode materials in ECs due to their accessibility, chemical stability, and variety of structures for diverse carbon materials, which always display relative low power density and/or energy density, as well as unsatisfied recycling durability.[12] more importantly, the harmful or expensive precursors, complex preparation process maybe involved in the syntheses，therefore limiting large-scale production for practical industry application.

As far as we know that, the storage energy performances of carbon based ECs are generally determined by the adsorption of electrolyte ions on large specific surface area of conductive electrodes, in which the surface charge is separated at

electrode/electrolyte interface. Therefore, high specific surface areas and pores adapted to electrolyte ion sizes are essential for ECs.[13-15] In particular, unique porous sheet-like carbon materials rather than graphene can serve as high-active electrodes due to high accessible surface area and thus greatly shorten the ion/electron transport length.[16] Unfortunately, even the most economically produced graphene-like material is nowhere near cost competitive with biomass-derived carbons achieved via simple pyrolysis or hydrothermal methods.[17-18] It should be pointed out, biomass would easily become one of ideal carbon candidates (c. a. activated carbon, carbon fiber, carbon paper and graphene products) via green chemical synthesis processes.[19-24]

Remarkably, regarding the porous carbon electrode materials originated from biomass has made great progress recently. For example, Li et al.[25] reported that porous carbon directly derived from the carbonization of sodium alginate exhibits excellent storage energy performances. Wang et al. prepared interconnected carbon nanosheets from the hemp and displays high specific capacitance of 144 F g^{-1} at a large current density of 100 A g^{-1}.[26] in addition, literature reported that sponge-like carbonaceous hydrogels and their ECs can be obtained via facile hydrothermal carbonization of watermelon biomass.[27] Qian et al. prepared flake-like carbons via 800 ^{o}C carbonization of human-air and deliver specific capacitance of 340 F g^{-1} at 1 A g^{-1} in 6 M KOH.[28] Wu et al.[15b, 18b] prepared starch derived carbon based microspheres via simply simultaneous template method and serve as excellent electrode materials. These results full demonstrated their potential advantages of the carbon based electrode materials from biomass in energy storage fields.

Chitosan (CS) is the naturally unique alkaline polysaccharide that composed of β-1,4-linked glucosamine.[29] Recently, CS has been extensively applied in such as biosensing, pharmaceutical, catalytic and separation fields due to its excellent biocompatibility, bioactivity, nontoxicity, adsorption performance, potent antimicrobial activity and low-cost.[30-33] In particular, it is easily obtained by N-deacetylation of the natural polymer of chitin and most abundant natural polymer cellulose.[34] Remarkably, the presence of plentiful amino and hydroxyl groups in the macromolecular chains is highly advantageous for conducting modification reactions and providing distinctive functions,[35] which can be highly facilitate the activation of chitosan and processing into high-performance materials with advanced functionalities.[36, 37] To our knowledge, regarding the synthesis of partially graphitic flake-like carbon based composites that derived from CS was seldom reported presently. As a result, developing a low-cost, green synthetic approach to synthesis of high-performances carbon-based electrodes still remains a great challenge.

In this study, we present that partially graphitic flake-like carbon based iron oxide composites were prepared via simple hydrothermal reaction followed by a high-temperature carbonization processes, detailed preparation process can be seen in Scheme 1. The prepared flake-like carbon/iron oxide composites serve as electrode in ECs and exhibit high specific capacitance and excellent recycling stability. More importantly, the specific synthetic approach for the unique flake-like carbons and their magnetic composites from CS would highlight their potential in such as energy storage, catalytic and environmental engineering fields.

Experimental Sections:

All reagents used were of analytical grade. The chitosan from crab shells was purchased from Sigma Aldrich, Iron(Ⅲ) nitrate and glacial acetic acid were purchased from Jinhua Chemical reagent company.

Preparation of Flake-like Carbon/Fe_3O_4 composite: In a typical synthesis, first, 0.15 g chitosan directly dissolve in 10 mL (0.1M) of acetic acid solution with magnetic stirring for 1 h to obtain homogeneous emulsion-transparent solution. The resultant solution became gelatinous at low temperature condition for several hours, then, the frozen samples were dried by lyophilization. The obtained precursor was transferred into 800 °C tubular furnace for 2 h at a heating rate of 5 ^{o}C min^{-1} under nitrogen atmosphere, and then naturally cooled to room temperature. Finally, black carbon powder was obtained. Similarly, 0.08 g $Fe(NO_3)_3.9H_2O$ is dissolved in 10 mL H_2O, then adding 0.1 g chitosan and 1 mL acetic acid into the above solution. The mixture was stirred vigorously for 1 h to form a homogeneous solution and then sealed in a 30 mL Teflon-lined stainless-steel autoclave. The autoclave was heated at 120 ^{o}C oven for 10 h, and allowed to cool to room temperature. The following treatment procedure is almost the same as that described above. Finally, black product can be obtained.

Characterization: Powder X-ray diffraction patterns were obtained in a Bruker AXS-D8 powder diffractometer in use of Cu-Kα (λ = 0.15405 nm) radiation. FTIR spectra were recorded with Bruker EQUINOX-55 infrared spectrophotometer on KBr pellet. The thermogravimetry analysis (TGA) was carried out on a Rigaku standard TG-DTA analyzer with a heating rate of 10 °C min^{-1} under nitrogen atmosphere. The

morphology of the samples was observed by scanning electron microscope (SEM, TM3000). Samples morphology/structure was observed by a FEI Quanta-400 FEG scan electron microscope (FE-SEM) with accelerating voltage of 20 KV. The structural and composition analysis were taken via using high-resolution transmission electron microscopy (Philips Tecnai G2 F20) at 200 kV that equipped with energy-dispersive spectroscopy (EDS). X-ray photoelectron spectroscopy (XPS) was conducted using Model VG ESCALAB apparatus with an Al Kα x-ray source to analyze the surface composition of the samples. The porous features of the prepared samples are determined by Brunaur–Emmett–Teller (BET) surface analyzer (Tri Star-3020, Micromeritics, USA). Prior to the measurements, all samples were degassed at 573 K until a stable vacuum of ca. 5 mTorr was reached. The Raman spectra was taken via using a Raman spectrometer (Jobin Yvon Co., France) model HR800 employing a 10 mW helium/neon laser at 632.8 nm.

Electrochemical Performances Measurement*:* All electrochemical evaluation was carried out using an electrochemical working station (CHI660E, Shanghai, China) in a three-electrode cell system at room temperature. The working electrode is fabricated by mixing the as-prepared pyrolysis products samples (8 mg) with carbon black (super-P-Li) and polyvinylidene difluoride (PVDF) at a weight ratio of 8:1:1. After thorough mixing, the slurry is pressed onto a piece of Nickel foam and then dried at 60 °C in a vacuum oven overnight (The effective area of the electrode is around 1.5 cm^2). All electrochemical measurements were carried out at room temperature in a three-electrode system consisting of the carbon based powder electrode as working

electrode, Saturated calomel electrode (SCE) as reference electrode, and a platinum wire electrode as counter electrode, respectively. The used electrolyte was 2 M KOH solution. Cyclic voltammograms (CV) was conducted within a potential ranged from -1.2 to -0.6 V versus SCE at various scan rates. The constant current charge-discharge testing was carried out at different current densities within a potential window from -1.2 to -0.6 V. The recycling lifetime testing was performed at current density of 1 A g^{-1}.

Results and discussion:

Herein, a kind of plate-like chitosan sample can be formed via simple immersion in 0.1 M ice-acetic acid solution for 12 h and followed by a freeze-drying treatment, as shown in Figure 1a. These plate-like structures are interconnected and form dense network-like aggregates. By further calcination at 800 ^{o}C furnace for 2 h, then, a class of flake-like patches was obtained, as shown in Figures 1b-c. further TEM observation find that the unique flake-like structure is actually composed of many smaller size patches and some hollow circles (Figure 1d). Herein, it was found from HRTEM image that these so called hollow circles display well-resolved crystalline stripe feature, the spacing is measured to be 0.34 nm, which is well coincided with the spacing of graphitic carbon material,[9] indicating highly graphitic characters, result was shown in Figure 1e. In addition, we perform Raman spectra measurement for the high-temperature sintered chitosan, as shown in Figure 1f. It was observed that there occur two obvious absorption peaks at approximately 1335 and 1568 cm^{-1}, respectively, which well correspond to the characteristic Raman peaks of

conventional carbon material,[38] confirming the formation of pure carbon species at present condition.

Meanwhile, a kind of carbon/iron oxide complex intermediate can be formed via 180 ^{o}C hydrothermal reactions for 12 h, as shown in Figure 2a, it was observed that numerous particles are dispersed on the surface of carbon substrate, additionally; the formed intermediate sample displays amorphous phase (data not shown), indicating present reaction temperature is not enough for achieving crystalline product. As a result, we perform further high-temperature carbonization for the prepared intermediate at 800 ^{o}C furnace for 2 h under N_2 atmosphere condition. Then, it was clearly found that numerous particles are well deposited onto the surface of the formed flake-like carbon support, as shown in Figure 2b. Further magnified SEM observation find that these particles are highly wrapped by the flake-like carbon materials, these particles have a mean size of approximately 1 μm, as shown in Figure 2c. Moreover, the particle can be assigned to be pure cubic-phase Fe_3O_4 according to standard JCPDS card no.75-0449, result was shown in Figure 2g, the present XRD pattern indicates the formed Fe_3O_4 product possess good crystalline feature. In addition, we further observe that Fe_3O_4 particles are well dispersed on the surface of the flake-like carbon substrate via TEM image, as shown in Figure 2d. At the same time, these flake-like carbon support displays well-resolved crystal lattice stripe, its spacing was 0.34 nm, implying certain graphitic feature (Figure 2e). Further HRTEM investigation reveals that the Fe_3O_4 particle exhibits good crystal lattice stripe, the spacing was measured to be 2.52 Å, correspond to (311) plane (Figure 2f).

Particularly, the Fe_3O_4 displays high-quality single-crystalline feature according to the electron diffraction (ED) pattern, as shown in Figure 2f (inset). Furthermore, we conduct the energy dispersive spectroscopy (EDS) testing for the sintered sample; it was found that the only presence of Fe, O and C elements in present sample, indicating the formation of pure carbon/ iron oxide product, as shown in Figure 2h.

The isothermal N_2 adsorption-desorption analysis was performed to further evaluate the porous features of specific flake-like carbon/Fe_3O_4 composite product. The N_2 adsorption-desorption isotherm at 77 K and Barrett-Joyner-Halenda (BJH) adsorption pore size distribution plot of the as-prepared sample is observed in Figure 3A. The nitrogen adsorption isotherm is a typical IV type curve. Additionally, we can confirm that the prepared carbon/Fe_3O_4 composite displays specific mesoporous feature according to the loop nature of the nitrogen adsorption isotherm. The specific BET surface area for the as-prepared carbon/Fe_3O_4 composite is measured to be 272.5 m^2 g^{-1}. In addition, according to the corresponding Barrett-Joyner-Halenda (BJH) pore size distribution curve, the pore size is measured to be 4.0 nm, as shown in Figure 3A (inset), which maybe resulted from the thermal-decomposition of CS at high-temperature condition.

Furthermore, the thermal stability of the as-synthesized carbon/Fe_3O_4 composite was investigated by TG analysis technique under N_2 atmosphere (Figure 3B). The first part weight loss was measured to be 48.1 wt. % when the temperature was changed from 287 to 500 ^oC, corresponding to the thermal-decomposition of the chitosan and part oxidation of the iron complex intermediate. Moreover, the second part weight

loss was measured to be 9.8 wt. % while the temperature was ranged from 500 and 800 ^{o}C, which could be ascribed to the full decomposition and carbonization of chitosan at higher temperature condition.

In order to investigate the element complex state of the samples, X-ray photoelectron spectroscopy (XPS) were performed for the carbon/Fe_3O_4 sample, as shown in Figure 4. The XPS spectrum in Figure 4a indicates the characteristic peak of O1s was centered at approximately 531 eV, confirming the presence of O oxidation valence state. XPS spectra of Fe2P (Figure 4b) shows two characteristic peaks that centered at approximately 724.6 and 710.7 eV, which are attributed to the Fe2P1/2 and Fe2P3/2, respectively. In addition, it is well known that the binding energy of element increases with the increase of its valence state. And the binding energy of Fe 2P3/2 is about 709 eV for Fe^{2+}, and 712 eV for Fe^{3+}.[39] Figure 4b shows the XPS signals of the Fe 2P1/2 and Fe 2P3/2 peaks, which indicates that both Fe^{2+} and Fe^{3+} should be coexisted showing the formation of Fe_3O_4.

On the other hand, the Fourier transform infrared (FTIR) spectra of the prepared samples were measured at room temperature (Figure 5). It was found that broad and strong peak at around 3400 cm^{-1} was produced from the *v*(O-H) stretching vibration mode, which suggests that the O-H of the carboxylate groups is partly deprotonated. In which, it was observed that the peak at approximately 3128 cm^{-1} corresponds to the bending vibration mode of -NH. The peak at 2920 cm^{-1} corresponds to the vibration mode of $–CH_2$ group. The peak at 2361 cm^{-1} can assign to the vibration mode of C-C bond. The characteristic peaks of C=O group were centered at approximately 1625

and 1287 cm^{-1}, respectively. The peak at 1494 cm^{-1} can assign to the stretching vibration mode of C-N bond. The strong peak at approximately 1400 cm^{-1} was assigned to the bending vibration mode of –C-H group. In addition, the peak at 1087 cm^{-1} can be assigned to C-O vibration mode. Additionally, the peak centered at 812 cm^{-1} was assigned to the out-plane bending vibration of O-H group. The strong peak at 673 cm^{-1} corresponds to vibration mode of the Fe-O bond.

It was known that, the porous features of the electrode are critical to facilitate the mass transport of electrolytes within the electrodes for fast redox reactions and double-layer charging/discharging. In which, we investigate the electrochemical performances for the prepared carbon-based electrodes in 2 M KOH solution. The electrochemical performances of the prepared flake-like carbon based electrodes were measured via a cyclic voltammetry (CV) technique. The typical CV curves for the obtained flake-like carbon electrode in 2 M KOH at different scan rates of 5, 10, 20, 50 and 100 mV s^{-1} are shown in Figure 6A, then, the achieved specific capacitances are 166, 150, 125, 81 and 48 F g^{-1}, respectively. In addition, galvanostatic charge-discharge measurements were carried out in 2 M KOH electrolyte via SCE at various current densities that ranged from 0.5 to 10 A g^{-1}, as shown in Figure 6B, then, the measured specific capacitances are 193, 180, 153, 130 and 80 F g^{-1} when applied current densities are 0.5, 1, 2, 5 and 10 A g^{-1}, respectively, result was shown in Figure 6C, indicating quick ion transport and low interfacial polarization. To further investigate the structural stability of flake-like carbon based electrode, we perform the recycling lifetime testing, as shown in Figure 6D. It was found from Figure 6D that

the specific capacitance retention was almost 100 % after 2000 cycles at current density of 1 A g^{-1}, implying the excellent recycling durability.

Meanwhile, the capacitive performances of the prepared graphitic carbon/Fe_3O_4 composite electrode were measured via a cyclic voltammetry (CV) technique. The typical CV curves for the carbon/Fe_3O_4 composite based electrode in 2 M KOH electrolyte at different scan rates of 5, 10, 20, 50 and 100 mV s^{-1} are shown in Figure 7A. Wherein, the lack of symmetry of the rectangle curve is found due to their pseudocapacitance behavior of Fe_3O_4 species. The pseudocapacitance reaction mechanism of Fe_3O_4 originates from the redox reaction on the surface of the flake-like carbon support; which can be further evidenced from the distinct redox peaks appeared in five CV curves. Additionally, it was observed that the reduction peaks of the entire curves take place negative shift with the increase of the scan rates. As for Fe_3O_4, two redox peaks at -1.0 and -0.7 V via SCE were clearly observed. The anodic wave centered at about -0.7 V via SCE represents the active dissolution of the iron electrode, which may be associated with the generation of ferrate. The formation of ferrate during the anodic scan is confirmed by the observation of a cathodic wave which occurred between -0.8 and -0.6 V, which corresponds to the reduction of iron (VI) to iron (III). The overall electrochemical behavior is in agreement with previous literature data.[40,41]

In addition, to further evaluate the application potential of the carbon/Fe_3O_4 composite as an electrode in ECs, galvanostatic charge-discharge measurements were carried out in 2 M KOH electrolyte at various current densities that ranged from 0.5 to

10 A g^{-1}, as shown in Figure 7B. The observation of nearly symmetric potential-time curves at all current densities implies the high charge-discharge columbic efficiency and low interfacial polarization of the unique electrode, as further evidenced in Figure 7D and F. This indicated that Fe_3O_4 species maybe suffer from reversible faradic redox reactions. Furthermore, we investigate the relationship between current density and specific capacitance, as shown in Figure 7C, it was found that the measured specific capacitances are 299, 256, 228, 220 and 131 F g^{-1} at current densities of 0.5, 1, 2, 5 and 10 A g^{-1}, respectively, which are superior to that previously reported carbon based composite electordes.[11, 42] This full demonstrate the graphitic flake-like carbon support can improve the electric conductivity of the composite electrode, additionally, high crystallization of Fe_3O_4 particle can provide additional pseudocapacitance and favor the stabilization of specific capacitance of the carbon/Fe_3O_4 composite electrode.[26] More importantly, the porous flake-like carbons not only contribute to high conductivity, but also enlarge the surface area of the whole electrode. Also the porous structure of the flake-like carbon provides more surface area in contact with the electrolyte, so more activated materials can effectively contribute to the capacitance. In addition, the outer accessible surface for activated material is completely utilized for charge storage at high rates.

Remarkably, to further investigate the capacitive performances of the prepared composite electrode, the recycling charge-discharge testing was performed. It was found that the electrode does not undergo obvious dramatically capacitance fading during the whole recycling process (Figure 7D). The specific capacitance retention

was measured to be 83 %, the specific capacitance can still retain to 215 F g^{-1} after 2000 cycles at current density of 1 A g^{-1}, indicating highly structural stability of the carbon/Fe_3O_4 composite electrode. Additionally, Figure 7E shows the correlation plot as a function of power density & energy density of the carbon/Fe_3O_4 composite electrode material. Then the formed electrode material can deliver a high energy density of ~ 135 Wh kg^{-1} at a power density of ~1598 W kg^{-1}, which are also superior to previously reported results in literatures,[43] implying its great advantages in high-performances storage energy devices.

Conclusions:

In summary, we first demonstrate a kind of graphitic flake-like carbon/Fe_3O_4 magnetic composite was produced via simple hydrothermal reaction followed by a high-temperature carbonization process. The prepared carbon-based samples display partially graphitic and well-defined porous feature. The electrochemical testing results demonstrate that the obtained carbon/Fe_3O_4 composite as electrode can deliver high specific capacitance of 299 F g^{-1} and excellent recycling stability. This case would be ascribed to the synergistic effects between the specific porous features of graphitic carbon support and the provided pseudocapacitance from Fe_3O_4 species. In general, the present synthetic approach is controllable and environmental-friendly, which can facilitate to prepare other advanced functional materials with specific surface textures.

ACKNOWLEDGMENT

We acknowledge the funding support from the National Science Foundation of China (NSFC) (No. 21001087, 21173167), the Education committee of Shannxi Province (Grant No.2010JK870, 2010JS115), Program for New Century Excellent Talents in University (NCET-13-0953), the Science and Technology Committee of Shannxi Province (Grant No. 2014KW09-03). We also thanks Dr. Xuemei Zhang in revision of References of the manuscript.

References :

1 a) J. R. Miller, A. Burke, *Electrochem. Soc. Interface*. **2008**, *17*, 53; b) T. Y. Wei, C. H. Chen, H. C. Chien, S. Y. Lu, C. Hu, *Adv. Mater*. **2010**, *22*, 2387; c) J. R. Miller, P. Simon, *Science* **2008**, *321*, 651; e) M. D. Stoller, R. S. Ruoff, *Energy Environ. Sci*. **2010**, *3*, 1294.

2 a) P. J. Hall, M. Mirzaeian, S. I. Fletcher, F. B. Sillars, A. J. R. Rennie, G. O. Shitta-Bey, G. Wilson, A. Cruden, R. Carter, *Energy Environ. Sci*. **2010**, *3*, 1238; b) S. W. Lee, B. M. Gallant, H. R. Byon, P. T. Hammond, S. H. Yang, *Energy Environ. Sci*. **2011**, *4*, 1972; c) G. Lota, K. Fic, E. Frackowiak, *Energy Environ. Sci*. **2011**, *4*, 1592.

3 a) Y. H. Lin, T. Y. Wei, H. C. Chien, S. Y. Lu, *Adv. Energy Mater*. **2011**, *1*, 901; b) C. Z. Yuan, X. G. Zhang, L. H. Su, B. Gao, L. F. Shen, *J. Mater. Chem*. **2009**, *19*, 5772; c) B. Wang, T. Zhu, H. B. Wu, R. Xu, J. S. Chen, X. W. Lou, *Nanoscale* **2012**, *4*, 2145.

4 a) P. Simon, Y. Gogotsi, *Nat. Mater*. **2008**, *7*, 845; b) P. Simon, Y. Gogotsi, *Acc. Chem. Res.* **2013**, *46*, 1094.

5 a) E. Frackowiak, *Phys. Chem. Chem. Phys*. **2007**, *9*, 1774; b) Y. Wang, Z. Shi, Y. Huang, Y. Ma, C. Wang, M. Chen, Y. Chen, *J. Phys. Chem. C*. **2009**, *113*, 13103.

6 a) Y. Gogotsi, P. Simon, *Science* **2011**, *334*, 917; b) L. Zhang, X. Yang, F. Zhang, G. K. Long, T. F. Zhang, K. Leng, Y. Huang, Y. F. Ma, M. Zhang, Y. S. Chen, *J. Am. Chem. Soc. 2013*, *135*, 5921.

7 G. H. An, H. J. Ahn, *Carbon* **2013**, *65*, 87.

8 N. A. Vacirca, J. K. Mcdonough, K. Jost, Y. Gogotsi, T. P. Kurzweg, *Appl. Phys. Lett*. **2013**, *7*, 07731.

9 Z. B. Yang, J. Deng, X. L. Chen, J. Ren, H. S. Peng, *Angew. Chem. Int. Ed*. **2013**, *52*, 13453.

10 L. F. Chen, Z. H. Huang, H. W. Liang, W. T. Yao, Z. Yu, S. H. Yu, *Energy. Environ. Sci*. **2013**, *6*, 3331.

11 M. Li, W. Xu, M. J. Wang, Y. P. Liu, X. Guo, *J. Power Sources* **2014**, *248*, 465.

12 G. P. Wang, L. Zhang, J. Zhang, *Chem. Soc. Rev*. **2012**, *41*, 797.

13 a) M. P. Bichat, E. Raymundo-pinero, F. Beguin, *Carbon* **2010**, *48*, 4351; b) T. Wei, C. H. Chen, H. C. Chien, S. Y. Lu, C. Hu, *Adv. Mater*. **2010**, *22*, 347.

14 A. S. Arico, P. Bruce, B. Scrosati, J. M. Tarascon, W. Schalkwijk, *Nat. Mater*. **2005**, *4*, 366.

15 a) D. R. Rolison, L. F. Nazar, *MRS. Bulletin* **2011**, *36*, 486; b) M. Wu, P. Ai, M. Tan, B. Jiang, Y. Li, J. Zheng, W. Wu, Z. Li, Q. Zhang, X. He, *Chem. Eng. J*, **2014**, *245*, 166

16 Q. Wang, J. Yan, T. Wei, J. Feng, Y. M. Ren, Z. J. Fan, M. L. Zhang, X. Y. Jing, *Carbon* **2013**, *60*, 481.

17 a) K. S. Novoselov, A. K. Geim, S. V. Morozov, D. Jiang, Y. Zhang, S. V. Dubonos, I. V. Grigorieva, A. Firsov, *Science* **2004**, *306*, 666; b) A. K. Geim, K. S. Novoselov, *Nat. Mater*. **2007**, *6*, 183.

18 a) X. Y. Deng, J. Lee, C. J. Wang, C. Matranga, F. Aksoy, Z. Liu, *Langmuir* **2001**, *27*, 2146; b) M. Wu, J. Liu, M. Tan, Z. Li, W. Wu, Y. Li, H. Wang, J. Zheng, J. S. Qiu, *RSC. Advances*, **2014**, *4*, 25189

19 Z. Li, Z. Xu, X. Tan, H. Wang, C. M. B. Holt, T. Stephenson, B. C. Olsen, D. Mitlin, *Energy Environ. Sci*. **2013**, *6*, 871.

20 Y. S. Yun, S. Y. Cho, J. Shim, B. H. Kim, S-J. Chang, S. J. Baek, Y. S. Huh, Y. Tak, Y. W. Park, S. Park, H. J. Jin, *Adv. Mater*. **2013**, *25*, 1993.

21 M. Biswal, A. Banerjee, M. Deo, S. Ogale, *Energy Environ. Sci.* **2013**, *6*, 1249.

22 L. Zhang, F. Zhang, X. Yang, K. Leng, Y. Huang, Y. Chen, *Small* **2013**, *9*, 1342.

23 A. Olejniczak, M. Lezansak, J. Wloch, A. Kucinska, J. P. Lukaszewicz, *J. Mater. Chem. A* **2013**, *1*, 8961.

24 H. Yao, G. Zheng, W. Li, M. T. McDowell, Z. Seh, N. Liu, Z. Lu, Y. Cui, *Nano Lett*.

2013, *13*, 3385.

25 Y. Z. Li, X. Zhao, Q. Xu, Q. H. Zhang, D. J. Chen, *Langmuir* **2011**, *27*, 6458.

26 H. Wang, Z. Xu, A. Kohandehghan, Z. Li, K. Cui, C. M. B. Holt, J. K. Tak, A. O. Anyia, D. Mitlin, *ACS NANO* **2013**, *7*, 5131.

27 X. L. Wu, T. Wen, H. L. Guo, S. Yang, X. Wang, A. W. Xu, *ACS NANO* **2013**, *7*, 3589.

28 W. Qian, F. Sun, Y. H. Xu, L. Qiu, C. Liu, S. Wang, F. Yan, *Energy Environ. Sci*. **2014**, *7*, 379.

29 C. Chang, S. Chen, L. Zhang, *J. Mater. Chem*. **2011**, *21*, 3865.

30 P. Chen, H. Y. Hwang, T. Y. Kuo, F. H. Liu, J. Lai, H. J. Hsieh, *J. Med. Biol. Eng.* **2007**, *27*, 23.

31 K. V. H. Prashanth, R. N. Tharanathan, *Trends Food Sci. Technol*. **2007**, *18*, 117.

32 C. Chatelet, O. Damour, A. Domard, *Biomaterials* **2001**, *22*, 261.

33 F. L. T. Shee, J. Arul, S. Brunet, A. M. Mateescu, L. Bazinet, *J. Agric. Food Chem*. **2006**, *54*, 6760.

34 M. Rinaudo, *Prog. Polym. Sci*. **2006**, *31*, 603.

35 a) S. F. Wang, L. Shen, W. D. Zhang, Y. J. Tong, *Biomacromolecules* **2005**, *6*, 3067; b) Y. Li, D. Yuan, M. Dong, Z. Chai, G. Fu, *Langmuir* **2013**, *29*, 11770.

36 X. M. Yang, Y. Tu, L. Li, S. Shang, X. M. Tao, *ACS Appl. Mater&Interf*. **2010**, *2*, 1707.

37 J. D. Qiu, J. Huang, R. P. Liang, *Sensors Actuators B: Chemical* **2011**, *160*, 287.

38 X. Li, W. Xing, S. Zhuo, J. Zhou, F. Li, S. Z. Qiao, G. Lu, *Bioresource Technology* **2011**, *102*, 1118.

39 a) A. P. Grosvenor, B. A. Kobe, M. C. Biesinger, N. S. Mclntyre, *Surf. Interface. Anal*. **2004**, *36*, 1564; b) P. Li, E. Y. Jiang, H. L. Bai, *J. Phys. D: Appl. Phys*. **2011**, *44*, 075003.

40 M. D. Koninck, T. Brousse, D. Belanger, *Electrochim. Acta*, 2003, *48*, 1425.

41 A. Denvir, D. J. Pletcher, *J. Appl. Electrochem.* 1996, *26*, 815.

42 F. Meng, Z. Fang, Z. Li, W. Xu, M. Wang, Y. Liu, W. Wang, D. Zhao, X. Guo, *J. Mater. Chem. A* **2013**, *1*, 7235.

43 a) A. B. Deshmukh, M. V. Shelke, *RSC. Advance*, **2013**, *3*, **21390**; b) H. Li, S. Q. Liu, H. Huang, Z. Zhou, Y. H. Li, D. Fang, *Electrochimica Acta* **2011**, *58*, 89.

Figures:

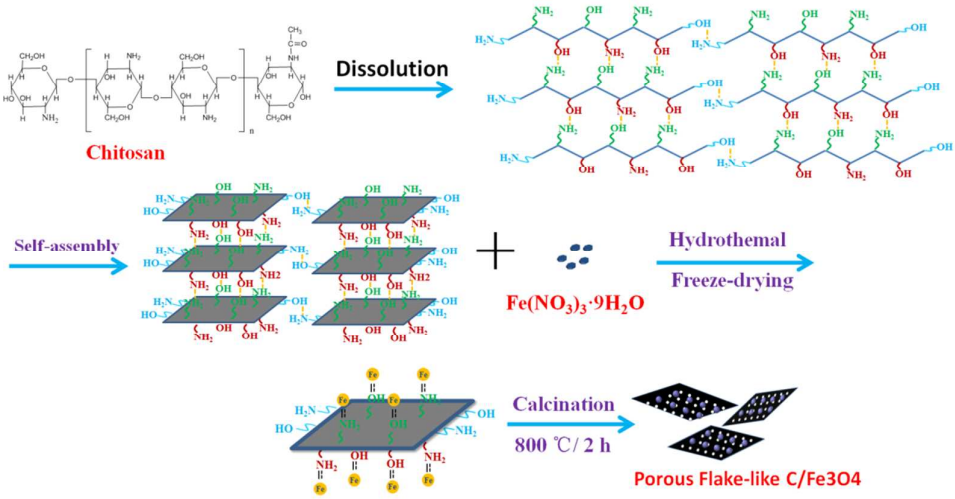

Scheme 1

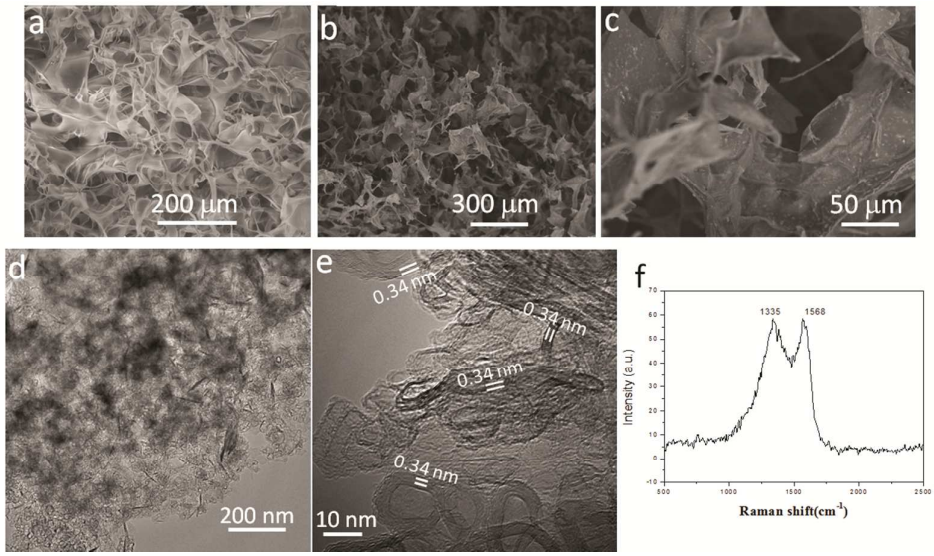

Figure 1

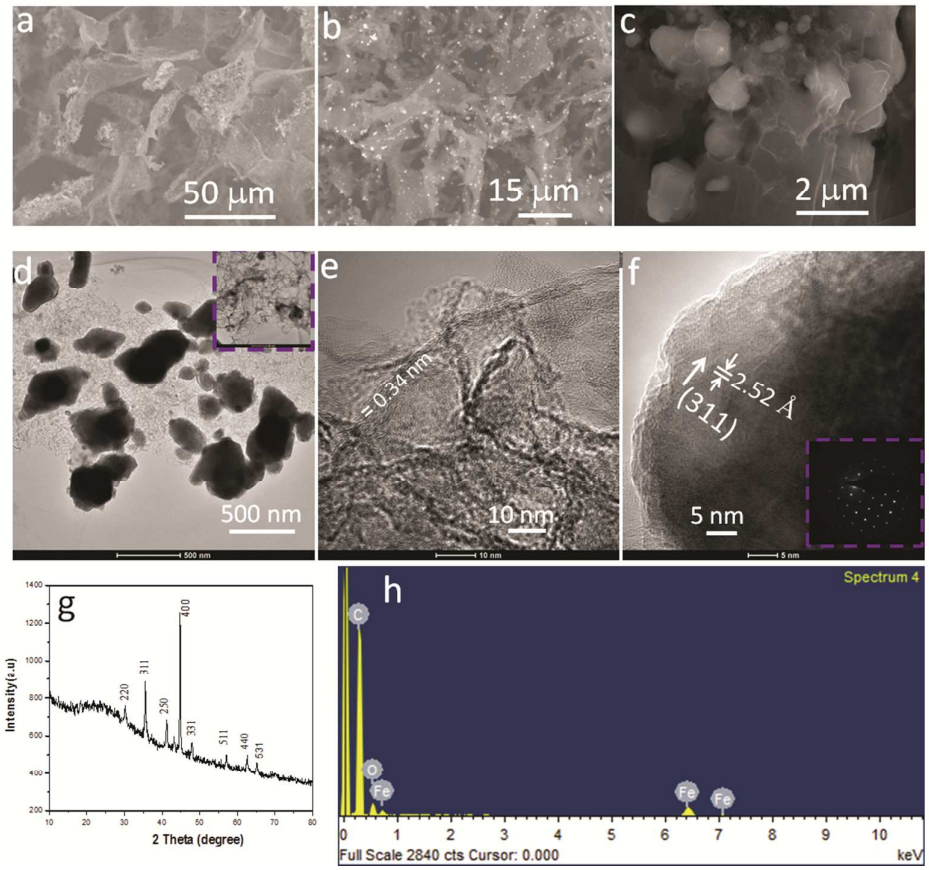

Figure 2

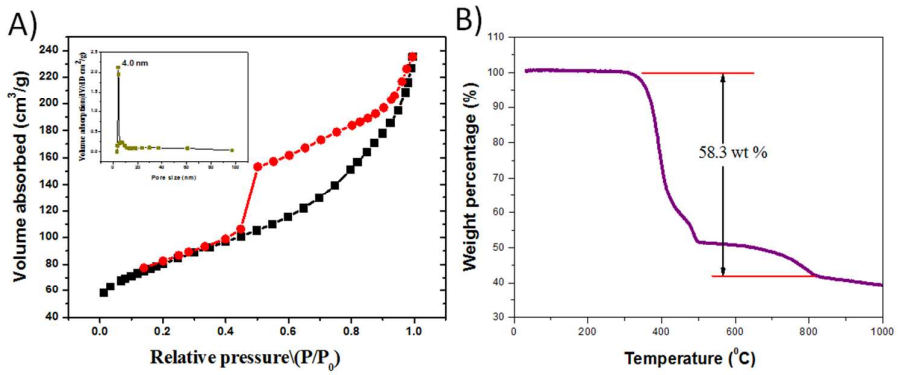

Figure 3

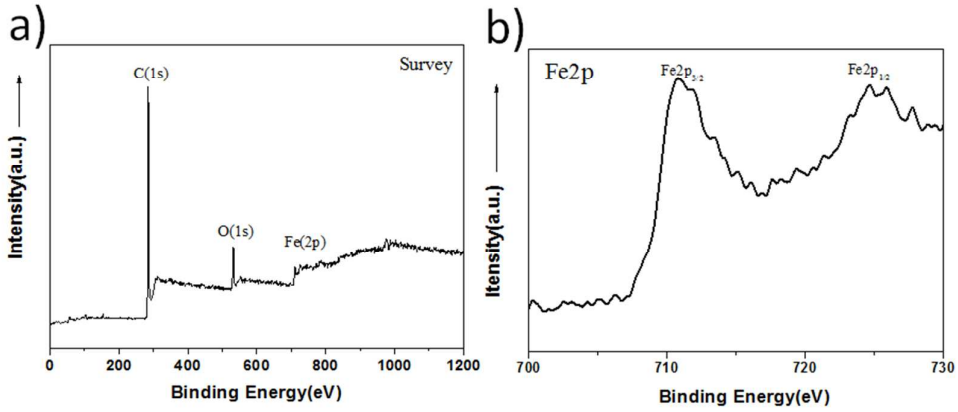

Figure 4

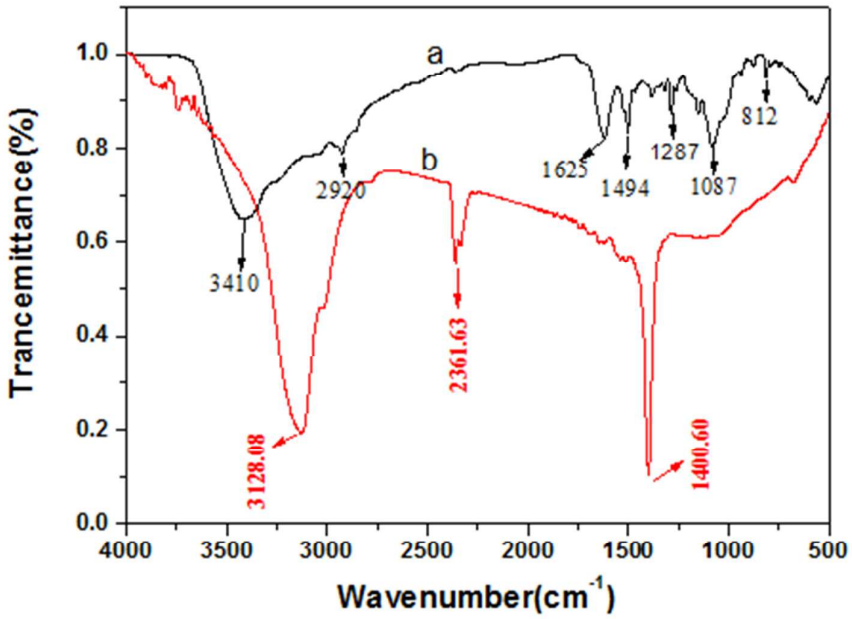

Figure 5

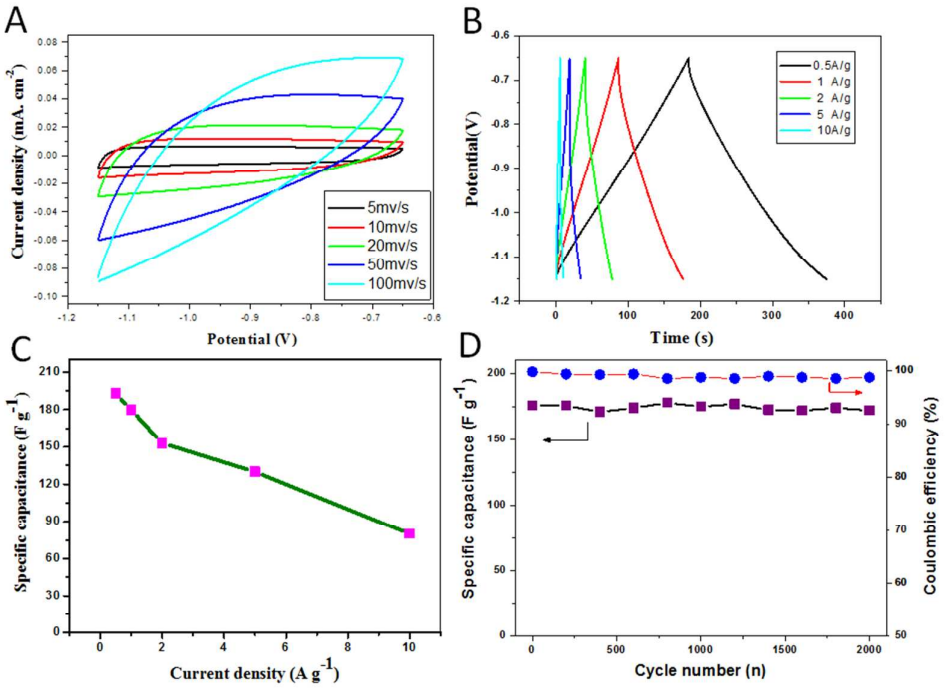

Figure 6

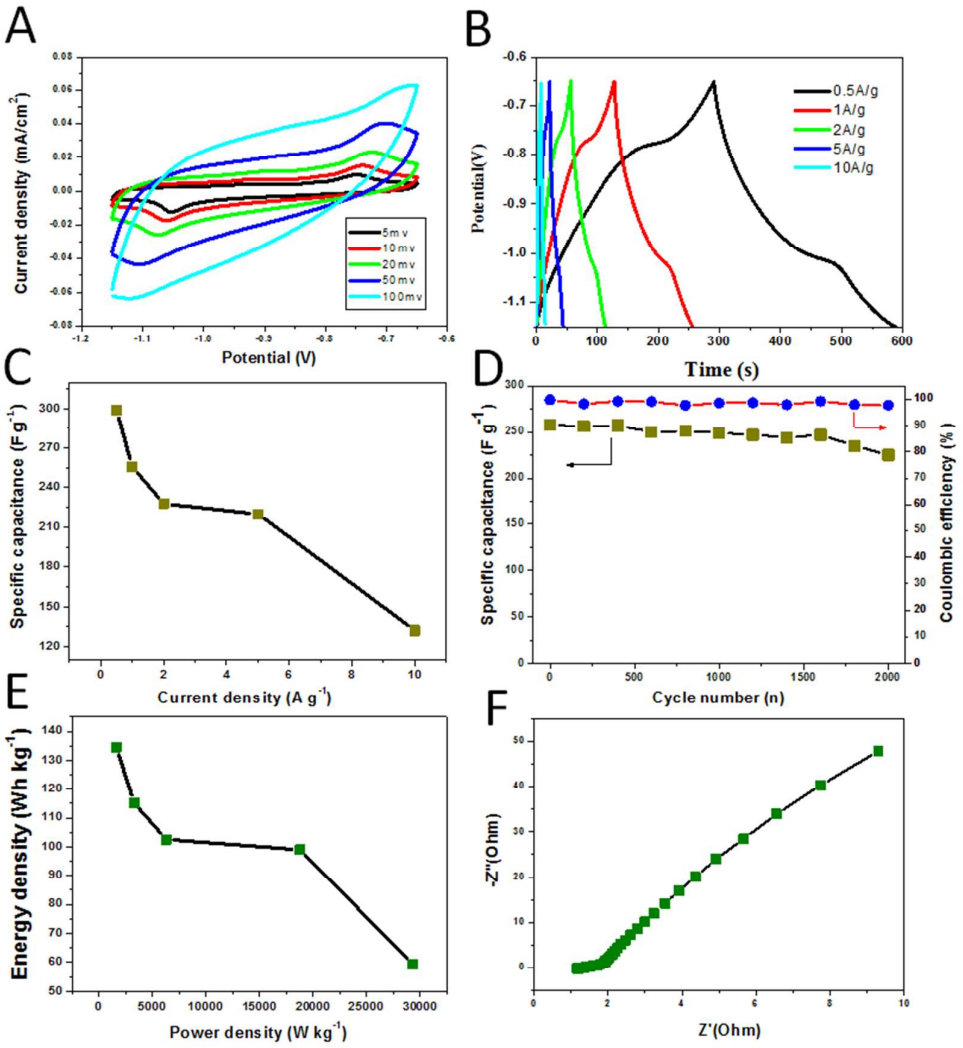

Figure 7

Captions:

Scheme 1: Illustration of the preparation process of the porous flake-like carbon/Fe_3O_4 composite.

Figure 1. Morphology and structure analysis for the prepared flake-like carbon based samples, a) SEM image of the pretreated chitosan material; (b-c) Low magnification SEM images; (d) TEM image; (e) HRTEM image: (f) Raman spectra of the carbonized product for pristine chitosan at 800 ^oC furnace for 2 h at N_2 atmosphere.

Figure 2. Morphology, structure and composition analysis for the graphitic carbon/ Fe_3O_4 composite, (a) SEM image of the carbon/iron oxide intermediate formed via 180 ^oC hydrothermal carbonization; (b-c) SEM images at different magnifications; (d) TEM image of the carbon/Fe_3O_4 composite; (e) HRTEM image for the underlying carbon substrate; (f) HRTEM image for the Fe_3O_4 component (inset is electron diffraction pattern); (g) XRD pattern; (h) EDS pattern for the prepared carbon/Fe_3O_4 at 800 ^oC furnace for 2 h calcination under N_2 atmosphere condition.

Figure 3: (A) Isothermal N_2 absorption/desorption curve (inset is pore-size-distribution curve); (B) TGA curve for the prepared porous flake-like carbon/Fe_3O_4 composite.

Figure 4. XPS spectra for the prepared carbon/Fe_3O_4 composite, a) survey spectra; b) XPS spectra of Fe2P species.

Figure 5: FTIR for the prepared samples, a) chitosan; b) carbon/Fe_3O_4 sample.

Figure 6: Electrochemical performances of the prepared flake-like carbon electrode, (A) cyclic voltammetry (CV) curves at various scan rates; (B) Charge/discharge curves at varying current densities; (C) correlation curve between current density and specific capacitance; (D) Recycling lifetime and Columbic efficiency curves at current density of 1A g^{-1}, the voltage windows were ranged from -1.2 to -0.6 V.

Figure 7: Electrochemical performances of the prepared carbon/Fe_3O_4 composite electrode, (A) cyclic voltammetry (CV) curve; (B) Charge/discharge curves at varying current densities; (C) Correlation curves between specific capacitances and various current densities; (D) Recycling lifetime and Columbic efficiency curves at current density of 1A g^{-1}; (E) the Plot as a function of power density &energy density; (F) Electrochemical impedance spectra (EIS) plots versus SCE, their voltage windows were ranged from -1.2 to -0.6 V.